LBL-15918
UC-37

Lawrence Berkeley Laboratory

UNIVERSITY OF CALIFORNIA

RECEIVED
LAWRENCE
BERKELEY LABORATORY

JUL 5 1983

LIBRARY AND
DOCUMENTS SECTION

Materials & Molecular Research Division

FAST, SELF-NULLING SPECTROSCOPIC ELLIPSOMETER: INSTRUMENTATION AND APPLICATION

R.H. Muller and J.C. Farmer

May 1983

TWO-WEEK LOAN COPY

This is a Library Circulating Copy which may be borrowed for two weeks. For a personal retention copy, call Tech. Info. Division, Ext. 6782.

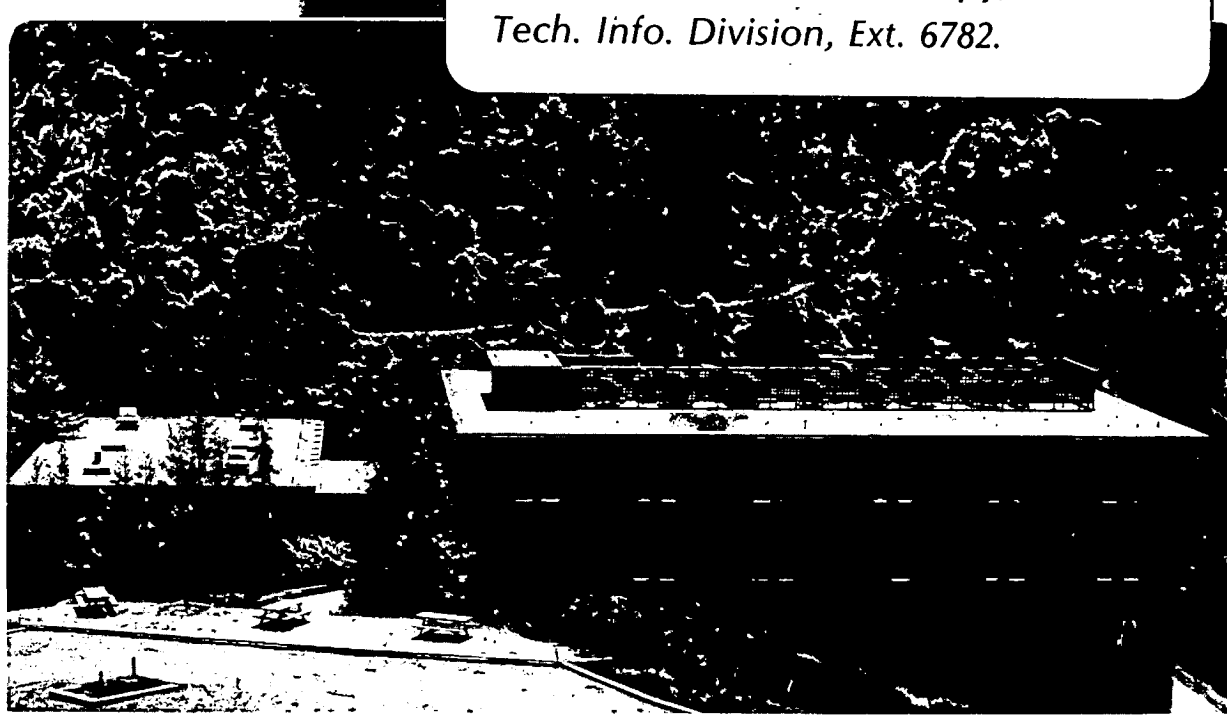

Prepared for the U.S. Department of Energy under Contract DE-AC03-76SF00098

LBL-15918 c.2

DISCLAIMER

This document was prepared as an account of work sponsored by the United States Government. While this document is believed to contain correct information, neither the United States Government nor any agency thereof, nor the Regents of the University of California, nor any of their employees, makes any warranty, express or implied, or assumes any legal responsibility for the accuracy, completeness, or usefulness of any information, apparatus, product, or process disclosed, or represents that its use would not infringe privately owned rights. Reference herein to any specific commercial product, process, or service by its trade name, trademark, manufacturer, or otherwise, does not necessarily constitute or imply its endorsement, recommendation, or favoring by the United States Government or any agency thereof, or the Regents of the University of California. The views and opinions of authors expressed herein do not necessarily state or reflect those of the United States Government or any agency thereof or the Regents of the University of California.

LBL-15918

FAST, SELF-NULLING SPECTROSCOPIC ELLIPSOMETER: INSTRUMENTATION AND APPLICATION

Rolf H. Muller and Joseph C. Farmer

Lawrence Berkeley Laboratory
Materials and Molecular Research Division
and
Department of Chemical Engineering
University of California, Berkeley
Berkeley, California 94720

ABSTRACT

The advantages of rapid spectral scanning have been combined with the inherent accuracy of a compensating ellipsometer operated in the polarizer-compensator-sample-analyzer configuration. Wavelength is varied over the visible-UV (370-720 nm) at a maximum rate of 114 nm/s by rotating a continuously-variable interference filter. A three-reflection Fresnel rhomb serves as the achromatic quarter-wave compensator. A microcomputer is used to collect spectroscopic measurements, perform instrument calibrations, digital filtering and interpret data. Wavelength-independent parameters of multiple-film optical models have been determined by treating measurements of delta and psi at different wavelengths as independent measurements. Experimental and predicted ellipsometer measurements are compared by use of statistical techniques for the determination of optimum values and confidence limits of model parameters.

Introduction

Spectroscopic ellipsometry can be used to determine structure and composition of thin films. For instance, Aspnes, et al. (1) have determined the microroughness of fine-grained polycrystalline and amorphous silicon films. They found that the microroughness, or micromorphology, can be accurately modeled as an equivalent film using either the Bruggeman or Maxwell-Garnett effective medium theories. In this study, spectroscopic ellipsometry has been used to determine the micromorphology of electrochemically deposited thin films of Pb on Cu. Several different optical models were investigated for the interpretation of the measurements, and a multilayer model was found to give best agreement with measurements.

Extensive modification of a self-compensating ellipsometer built previously (2) and based on principles proposed earlier by Layer (3), has made it possible to combine rapid spectral scanning with the inherent accuracy (4) of compensating measurements.

Optical Components

The ellipsometer employs the polarizer-compensator-sample-analyzer configuration, the arrangement of optical components is shown schematically in Fig. 1. Collimated monochromatic light is linearly polarized by a Glan-Thompson prism (polarizer). An achromatic quarter-wave retarder (compensator) produces elliptically polarized light incident on the sample surface. After reflection the light is linearly polarized and can be extinguished by a second Glan-Thompson prism (analyzer). A photomultiplier tube is used to measure the intensity of the light transmitted by the analyzer, after collection by a second telescope.

Azimuths of the transmission axes of polarizer and analyzer and the azimuth of the fast axis of the compensator are measured at compensation (extinction) and used to calculate the ellipsometer parameters, delta and psi (relative phase and amplitude).

The Faraday cells produce a magneto-optic rotation of the plane of polarization which is additive to the mechanical rotation of polarizer and analyzer prisms and is electronically controlled. Modulation currents of 10 kHz and 90 degree phase difference are applied to both Faraday cells, resulting in an oscillation of the effective polarizer and analyzer azimuths. Error signals derived from the response of the photomultiplier to about ten oscillations are generated by phase sensitive detection with integration and used to drive the effective polarizer and analyzer azimuths to compensation by control of the Faraday cell currents.

Spectral scanning is achieved by rotating a continuously-variable interference filter, positioned between a white light-source (75 W, current stabilized high-pressure Xe arc*) and the collimating telescope of the polarizer (Fig. 1). The maximum scan rate was 114 nm per second (1 pass through the spectral range every 3 seconds); lower noise levels can be achieved by use of a lower scan rate (23 nm per second or 1 pass through the spectral range every 15 seconds). The optical properties of this filter are given in Table I; as it revolves, the wavelength passed varies linearly from approximately 370 to 720 nm during the first half turn of rotation, and then decreases to 370 nm during the second half turn of rotation. A digital incremental encoder,** which is coupled to the rotation shaft of the filter with a flexible linkage, is used to measure

---

*Oriel C-72-20

**STRE-2014-010

angular position and, thus, wavelength. Transmitted wavelength has been calibrated in terms of angular position with known spectral lines. At present, the useful spectral range is limited by the absorption of the Faraday cells in the UV and the sensitivity of the photomultiplier in the near IR. Advantages of the interference filter over other types of monochromators include high transmittance, straight-through beam path, small space requirement (2.5 cm), continuous bidirectional spectral scanning (no discontinuities in wavelength upon continuous rotation) and lack of polarization. Since the spectrum is scanned twice in opposite directions during a single revolution of the filter, possible artefacts caused by filter imperfections or instrument response can be identified. The principal disadvantages of a continuously variable interference filter are the relatively broad bandwidth of the transmitted wavelength, (6 nm to 17 nm, see Table I) and the possible degradation of the filter coating with age.

The dependence of the effective Verdet coefficient (rotation per unit solenoid current) of the Faraday cell glass cores on wavelength has been determined experimentally and is shown in Fig. 2. Rotation of the analyzer and polarizer azimuths is linearly proportional to solenoid current over the entire dynamic range of the Faraday cells, which is $\pm$ 18° at 700 nm and $\pm$ 70° at 400 nm.

A three-reflection Fresnel rhomb with extremely low axial skew (<0 01 deg., Continental Optical Co.) has been used as the achromatic quarter-wave compensator However, imperfections in the fabrication of the device have required re-alignment before four-zone measurements could be conducted.

It was found that the photomultiplier previously used for ellipsometry at a fixed wavelength of 546.1 nm (RCA 931-A, range 300 to 650 nm, peak at 400 nm) had to be replaced to avoid the loss of signal in the red part of the spectrum. An "extended red" photomultiplier (Hammamatsu R-928, range 185 - 930 nm, peak at 400 nm) greatly improved the spectral scanning range. A gain-leveling circuit was incorporated into the Faraday cell controller to maintain wavelength-independent detector response, but its use was not normally required.

Computer System

The high rate at which ellipsometer data are generated during rapid spectral scanning requires the use of a digital data acquisition system.* The current passed through the polarizer and analyzer Faraday cell solenoids to produce nulling are monitored by the computer over two channels of an 8-channel analog-to-digital converter.** Faraday cell currents are converted post-experiment to analyzer and polarizer azimuths by taking into consideration the wavelength dependence of the specific rotation (effective Verdet coefficients); these azimuths are then converted to delta and psi. Wavelength, which varies linearly with the angular position of the filter, is monitored by counting pulses from the rotary incremental encoder. The encoder is interfaced to the computer via an addressable pulse counter. For each revolution the encoder generates an index pulse in one channel and 400 pulses in a second channel. Angular position is determined by counting the high-repetition pulses and using the index pulse to reset the count for every revolution; software interprets this count (0 to 400) as wavelength on the basis of calibrations.

*Digital LSI-11/2
**Datel MST-LSI2

The frequency of the high-repetition pulses is used as a measure of scan rate.

Digital filtering is done by averaging all data collected between encoder pulses. Sampling of channels was limited by the A/D conversion rate (about 1000 readings per second). Further noise reduction is possible by averaging several scans.

Data are periodically transferred from the buffer memory to double density floppy disks in unformatted form. To increase the storage efficiency of the disk, wavelengths are recorded in abbreviated form. Data can be displayed on the screen of a graphics terminal,* as high-quality output from a digital interactive plotter,** or as numeric output from a teletype.¶ The graphics terminal also serves as the control console of the instrument.

Electrochemical Film Deposition

Thin films of lead on copper substrates were prepared by potentiostatic deposition (-600 mV vs. Ag/AgCl) from an electrolyte consisting of 5 mM $Pb(NO_3)_2$ and 1 M $NaClO_4$ at a pH of 3. Details of the electrochemical cell are given elsewhere (5-7). Electrochemical film formation has the advantage that the amount of material deposited can be determined independently from the charge passed

Based upon charge passed, the film thicknesses would have been 31, 60 and 110 nm if the deposit had formed uniformly and had been compact.

*Digital VT 55
**Tektronix 4662
¶TT 43

However, it was found that the deposit was not homogeneous and compact, and multilayer optical models had to be used to explain the spectroscopic ellipsometer measurements.

Single-Layer Optical Models

Predictions based upon the following three optical models for single layer films (Fig. 3) were compared to experimental spectroscopic ellipsometer measurements. The first was a compact film model, in which the entire deposit was treated as bulk Pb and there was only one adjustable parameter, the deposit thickness. Figure 4 shows spectroscopic simulations of delta for various assumed thicknesses (solid lines labeled 0, 1, 5, 10 nm, etc.). Comparison with experimental measurements also shown on the figure (dotted lines for 31, 60, and 110 nm compact thicknesses) illustrates that this model is inadequate.

The second single-layer optical model was a porous film in which porosity was taken into consideration by use of an effective refractive index. Pores were treated as microinclusions of electrolyte in a Pb host medium and the optical properties of an isotropic homogeneous film were computed by use of the Maxwell-Garnett or Bruggeman equations. These equations have been used in the literature for modeling rough surfaces and particulate films (1, 8-10). The model involved two adjustable parameters, the deposit thickness and porosity. Spectroscopic simulations of the ellipsometer parameter delta for this model are shown in Fig. 5

for an amount of deposit corresponding to a 31 nm thick, compact Pb layer (based upon coulometric measurements) redistributed on a Cu substrate as deposits of various porosities. Simulations are represented by solid lines and experimental measurements are represented by dotted lines. It is evident that this model alone is also inadequate to explain experimental measurements of delta and deposit thickness based on charge.

The third model was based on the coherent superposition of polarization states resulting from reflection of adjacent film-covered and bare elements of a patchwise covered surface (11, 12). The island film may be compact, porous or anisotropic. In the latter case, at least six unknown film parameters would have to be determined, which results in unacceptable parameter variances. The dimensions of the islands are assumed to be smaller than the transverse and longitudinal coherence of the incident light at the specimen surface. For the spectroscopic ellipsometer, the longitudinal coherence ranges from 16 microns at 400 nm to 49 microns at 700 nm (13); the transverse (lateral) coherence ranges from 10 microns at 400 nm to 17 microns at 700 nm (14). These estimates assume (conservatively) a bandwidth twice that of the source (20 nm). Since complementary SEM studies of the films investigated here have shown the dimensions of dendritic islands to be less than 15 microns, the coherent superposition model is justified for the present experiments.

Spectroscopic simulations of delta for films corresponding to a 31 nm thick, uniform, compact Pb deposit (based upon coulometric measurements), redistributed on a Cu substrate as compact islands, are shown in Fig. 6. The island model used for these simulations employed two adjustable parameters, fractional surface coverage and island thickness. Combinations of these two parameters which were consistent with the amount of Pb known to be in the film from coulometric measurements were used. It can be seen that this model is also incapable of explaining the experimental measurements.

For all single-layer optical models, disagreement of the computed spectral dependence of psi was similar to that shown for delta. Note that interpretations of measurements at a single wavelength often appear possible, although the entire spectral range cannot be fitted.

Multiple-Layer Optical Models

A three-layer model is illustrated in Fig. 3d. The first layer was assumed to be an isotropic film representing the underpotential deposit. Optical properties of this layer were determined in a separate study (15).

The second layer was assumed to be a granular, porous deposit with optical constants computed from the properties of Pb and electrolyte, by use of the Bruggeman theory for a binary mixture, Eqs. 1-5. Incorporation of this layer into the optical model was motivated by light scattering measurements (5).

$$\frac{\hat{\varepsilon}_{Pb} - \hat{\varepsilon}_f}{\hat{\varepsilon}_{Pb} + 2\hat{\varepsilon}_f}\,\theta_{Pb} + \frac{\hat{\varepsilon}_s - \hat{\varepsilon}_f}{\hat{\varepsilon}_s + 2\hat{\varepsilon}_f}(1 - \theta_{Pb}) = 0 \qquad (1)$$

$$\hat{\varepsilon}_f = \frac{1}{2}\left[-\hat{A} \pm (\hat{A}^2 - 4\hat{B})^{1/2}\right] \tag{2}$$

$$\hat{A} = \frac{1}{2}\left[\hat{\varepsilon}_{Pb}(1-3\theta_{Pb}) + \hat{\varepsilon}_s\,(3\theta_{Pb} - 2)\right] \tag{3}$$

$$\hat{B} = -\frac{1}{2}\left[\hat{\varepsilon}_{Pb}\,\hat{\varepsilon}_s\right] \tag{4}$$

$$\hat{n}_f = \hat{\varepsilon}_f^{\,1/2} \tag{5}$$

The root with the largest modulus was used as solution of Eq. 1 (16).

The third layer represented dendritic Pb islands, visible in scanning electron micrographs, and was modeled by an island film and coherent superposition of polarization states (Eq. 6) resulting from reflection on adjacent surface elements with and without island coverage.

$$\hat{r}_\nu = \theta_f \hat{r}_{\nu,f} + (1-\theta_f)\hat{r}_{\nu,s} \tag{6}$$

Use of coherent superposition implies that the diameter of islands is smaller than the spacial coherence of the illuminating light. The total amount of Pb contained in the three layers was adjusted to agree with the coulometric measurements.

Although the three-layer model provides very good agreement between predictions and measurements, the computations have shown that the optical effect of the third (dendritic island) layer is often negligible, because the surface coverage by islands is small (5-10%). A simplified two-layer model was therefore used for interpretations. Only 3 unknown parameters have to be determined with this model (thickness of the first, compact layer, thickness and porosity of the second, porous layer) as opposed to six parameters required for the three-layer model. Despite the insignificant optical effect of the dendritic island layer, it usually contained about 2/3 of the Pb deposit known to be present from coulometric measurement. All optical constants were determined experimentally from independent measurements, and were not treated as adjustable parameters.

Optimization of the Two-Layer Model

Optimization of the wavelength-independent parameters required to specify only the first two layers resulted in smaller parameter variances than if all three layers were included. This strategy is based on the assumption that the third layer of islands has an insignificant optical effect. All deposited Pb not accounted for in the first two layers

after optimization was assumed to be distributed in the dendritic islands.

Results of the optimization are shown in Figs. 7 and 8 (delta and psi vs. wavelength). The solid lines represent experimental measurements and the circles represent points calculated by a multidimensional optimization routine. Very good agreement was obtained by optimization of the thickness and porosity of the second layer, which are wavelength-independent adjustable parameters. Table II summarizes the results of the optimization. Measured and calculated values of delta and psi at particular wavelengths are tabulated for three thicknesses. The amount of material, based on coulometric measurements, present in these films corresponds to compact layers of thickness 31, 60 and 110 nm. By minimizing the sum-of-squares error (17) between the model predictions and measured values of delta and psi over the entire spectral range, one determines the optimum values of the wavelength-independent adjustable parameters (thickness and porosity). Table II also gives the values of the sum-of-squares error, the thickness and porosity of the second layer with their statistically-determined confidence interval. Properties of the first compact layer are those of the underpotential deposit (5,15). Thicknesses and porosities of the second layer are thus found to be 31 nm and 41 percent; 50 nm and 22 percent; and 87 nm and 3 percent, respectively.

Equation 7 defines the sum-of-squares error for the model; the parameter variance is defined in Eq. 8.

$$S = \sum_{i=1}^{n} \left[(\Delta_{C,i}-\Delta_{M,i})^2 + (\Psi_{C,i}-\Psi_{M,i})^2\right]^{1/2} \qquad (7)$$

$$SE(p) = \frac{\sigma^2}{\frac{1}{2}\frac{\partial^2 S}{\partial p^2}} \qquad (8)$$

Parameter confidence intervals (Eq. 9) are calculated from this variance and the student t-statistic at a 95% confidence level for "2N-P" degrees of freedom, where "N" is the number of delta-psi measurements over the spectral range (from a single spectroscopic scan) and "P" is the number of adjustable parameters. Wavelengths of individual measurements are spaced at intervals greater than the source bandwidth; measurements at each wavelength are treated as independent observations of the same surface.

$$\delta(p) = t(2N-P,\ 1-2\alpha)[SE(p)]^{1/2} \tag{9}$$

Values of both numerator and denominator of Eq. 8 are required and are estimated by use of Eqs. 10 and 11, respectively

$$\sigma^2 = S_{MIN}/df = S_{MIN}/(2N-P) \tag{10}$$

$$\frac{1}{2}\frac{\partial^2 S}{\partial p^2} \sim \frac{S_{(+)} + S_{(-)} - 2S_{MIN}}{2(\Delta p)^2} \tag{11}$$

Note that the variance for any parameter increases dramatically as the total number of model parameters P approaches the number of data points (2N) used in the optimization

Conclusions

A novel fast spectral-scanning self-nulling magneto-optic ellipsometer, based on an earlier design has been built. The instrument is fully computerized.

Spectroscopic ellipsometry allows one to calculate confidence intervals of wavelength-independent parameters for micromorphological optical

models and to justify the use of more sophisticated optical models on the basis of the greater degrees-of-freedom.

For three electrolytically formed Pb deposits (compact thickness 31 nm, 60 nm, and 110 nm) the best agreement between measurements and model predictions was obtained for a three-layer model or a two-layer simplification of it. The distribution of deposited material between compact, porous (granular), and dendritic island layers could be determined.

Acknowledgments

This work was supported by the Director, Office of Energy Research, Office of Basic Energy Sciences, Materials Sciences Division of the U.S. Department of Energy under contract no. DE-AC03-76SF00098.

NOMENCLATURE

df	degrees of freedom, 2N-P
$\hat{n}_f$	complex refractive index of porous film
$\hat{r}_\nu$	complex Fresnel reflection coefficient for polarization ν (s or p)
$\hat{r}_{\nu,f}$	complex Fresnel reflection coefficient for film-covered surface
$\hat{r}_{\nu,s}$	complex Fresnel reflection coefficient for bare surface
t(2N-P, 1-2α)	student t-statistic for "2N-P" degrees-of-freedom at a "1-2α" level of confidence
$\hat{A}$, $\hat{B}$	complex parameters for quadratic equation
N	number of pairs of Δ and ψ measurements
P	number of model parameters to be fitted
SE(p)	variance of parameter p
S	sum-of-squares between measured and calculated delta ($\Delta_{M,i}$ and $\Delta_{C,i}$ respectively), and between measured and calculated psi ($\psi_{M,i}$ and $\psi_{C,i}$ respectively) summed over all i^{th} wavelengths
S_{MIN}	minimum value of $S_{\Delta,\psi}$ corresponding to a selection of optimum p values
$S_{(+)}$	value of S computed for the optimum parameter value plus Δp
$S_{(-)}$	value of S computed for the optimum parameter value minus Δp
α	level of confidence, 1-2α

$\delta(p)$	error in parameter "p" at a "1-2α" level of confidence
$\hat{\varepsilon}_f$	complex dielectric function of porous film
$\hat{\varepsilon}_{Pb}$	complex dielectric function of metallic Pb
$\hat{\varepsilon}_s$	complex dielectric function of electrolyte solution
σ^2	variance of model predictions for Δ and ψ
θ_f	fraction of surface covered by film of refractive index $\hat{n}_f$
θ_{Pb}	volume fraction of Pb in porous film
Δ	ellipsometer parameter, phase difference between p and s electric field components after reflection, relative to the incident (degrees)
$\Delta_{C,i}$	calculated value of Δ
$\Delta_{M,i}$	measured value of Δ
ψ	ellipsometer parameter, amplitude ratio of p and s electric field components after reflection (tan ψ), relative to the incident (degrees)
$\psi_{C,i}$	calculated value of ψ
$\psi_{M,i}$	measured value of ψ

References

1. D. E. Aspnes, J. B. Theeten and F. Hottier, Investigation of the Effective-Medium Models of Macroscopic Surface Roughness by Spectroscopic Ellipsometry, Phys. Rev.B, 20, 3292 (1979).

2. H. J. Mathieu, D. E. McClure and R. H. Muller, Fast Self-Compensating Ellipsometer, Rev. Sci. Instrum., 45, 798 (1974).

3. H. P. Layer, Circuit Design for an Electronic Self-Nulling Ellipsometer, Surf. Sci., 16, 177 (1969).

4. D. E. Aspnes, Precision Bounds in Ellipsometer Systems, Appl. Opt. 14, 1131 (1975).

5. J. C. Farmer and R. H. Muller, Nucleation of Pb Electrodeposits on Ag and Cu, submitted to J. Electrochem. Soc.

6. J. C. Farmer and R. H. Muller, The Effect of Rhodamine-B on Pb Electrodeposition on Ag and Cu, submitted to J. Electrochem. Soc.

7. J. C. Farmer, Effect of Organic Adsorbates on the Initial Stage of Electrolytic Metal Deposition: Development and Use of a Spectroscopic Ellipsometer, Ph.D. dissertation, Department of Chemical Engineering, University of California, Berkeley, Lawrence Berkeley Laboratory, LBL-15607, March 1983.

8. R. M. A. Azzam and N. M. Bashara, Polarization Characteristics of Scattered Radiation from a Diffraction Grating by Ellipsometry with Application to Surface Roughness, Phys. Rev. B, 5, 4721 (1972).

9. R. H. Muller and C. G. Smith, Use of Film Formation Models for the Interpretation of Ellipsometer Observations, Surf. Sci., 96, 375 (1980).

10. D. E. Aspnes and J. B. Theeten, Investigation of Effective-medium Models for the Interpretation of Ellipsometer Observations, Surf. Sci., 96, 375 (1980).

11. R. H. Muller, Principles of Ellipsometry in ADVANCES IN ELECTROCHEMISTRY AND ELECTROCHEMICAL ENGINEERING, Vol. 9, edited by C. W. Tobias and P. Delahay, Wiley, New York, 1973, p. 220.

12. C. G. Smith, Ellipsometry of Anodic Film Growth, Ph.D. Thesis, Department of Chemical Engineering, University of California, Berkeley, LBL-8082 (1978).

13. G. R. Fowles, INTRODUCTION TO MODERN OPTICS, 2nd ed., Holt, Rinehart, and Winston, New York, 1975, pp. 74-75.

14. M. Born and E. Wolf, PRINCIPLES OF OPTICS, MacMillan, New York, 1964, p. 551

15. R. H. Muller and J. C. Farmer, Macroscopic Model for the Ellipsometry of an Underpotential Deposit: Lead on Copper and Silver, submitted to Surf Sci.

16. W. Kahan, personal communication, Department of Electrical Engineering and Computer Science, University of California, Berkeley, August 1982.

17 G. E. Box and G. A. Coutie, Application of Digital Computers in the Exploration of Functional Relationships, Proc. Inst. Electr. Engrs., 103 B, Suppl. 1, 100 (1956)

Table I. Spectral Characteristics of the continuously variable interference filter monochromator (Optical Coatings Laboratory, Bonded CVF with 1 mm Slit)

Angular Position	Center Wavelength (1/2 PWR)	Wavelength Bandwidth (1/2 PWR)	Peak Transmission
degrees	nm	nm	percent
5	377.77	5.84	12.60
30	423.90	6.89	39.66
60	483.90	8.12	43.78
90	542.67	9.77	41.74
120	603.54	11.92	41.65
150	664.48	14.29	44.03
175	716.02	16.53	48.56
185	710.61	16.21	48.81
210	658.75	13.87	45.24
240	597.20	11.42	42.86
270	536.66	9.58	41.25
300	476.99	7.98	43.63
330	417.58	6.68	36.98
355	372.77	6.37	7.69

Table II. Spectroscopic Ellipsometry of Pb Deposits: Optimization of 2-Layer Model. Confidence Intervals for Model Parameters given for 95% Confidence Limits.

Amount of Deposit	30 nm				60 nm				110 nm			
Wavelength (Å)	Δ(deg) meas.	Δ(deg) calc	ψ(deg) meas.	ψ(deg) calc.	Δ(deg) meas.	Δ(deg) calc	ψ(deg) meas.	ψ(deg) calc.	Δ(deg) meas.	Δ(deg) calc.	ψ(deg) meas.	ψ(deg) calc.
4248	58.69	60.54	32.99	28.92	78.01	81.97	32.55	29.30	89.84	94.25	34.62	29.61
4492	57.24	56.49	31.12	31.68	76.02	75.64	30.14	31.60	88.42	87.64	31.81	31.76
4756	55.48	54.28	30.88	30.97	73.77	73.63	29.11	30.16	86.53	85.84	30.35	30.30
5155	52.73	51.89	30.99	30.90	71.42	71.19	28.81	29.18	84.44	83.69	29.42	29.32
5586	50.07	49.59	31.73	31.48	69.52	69.44	28.68	28.60	82.91	82.44	28.99	28.85
5998	49.97	49.81	33.58	33.50	66.95	66.71	29.04	28.70	81.14	80.88	28.84	28.77
6242	51.03	50.91	34.47	34.38	65.91	64.95	29.62	29.25	79.68	79.47	29.10	28.99
6504	51.85	52.27	35.35	35.24	64.99	63.54	30.59	30.38	78.06	77.90	29.85	29.71
6748	52.87	53.69	36.39	35.99	64.58	63.04	31.99	31.78	76.99	76.79	30.96	30.81
6991	53.45	55.14	38.11	36.89	64.09	63.12	34.33	34.53	75.53	75.30	33.65	33.52
MEAN SQUARES ERROR BETWEEN MEASURED AND CALCULATED Δ AND ψ (deg)	5.359				6.049				6.835			
THICKNESS OF POROUS LAYER (Å)	310 ± 41				500 ± 162				870 ± 2664			
VOL. FRACTION Pb IN POROUS LAYER	0.585 ± 0.139				0.775 ± 0.165				0.968 ± 0.274			
THICKNESS OF COMPACT LAYER (Å)	4.8 ± 1.1				4.8 ± 1.1				4.8 ± 1.1			

Figure Captions

Fig. 1. Spectral-scanning, self-nulling ellipsometer, optical components and electrical connections. 1. High pressure Xe lamp, 2. rotating interference filter, 3. collimator, 4. polarizer Glan-Thompson prism, 5. polarizer Faraday cell, 6. Fresnel rhomb achromatic retarder, 7. electrochemical cell, 8. analyzer Faraday cell, 9. analyzer Glan-Thompson prism, 10. collimator, 11. spectrally "flat" detector, 12. rotary incremental digital encoder, 13. spectral scanner drive motor

Fig. 2 Specific rotation (effective Verdet coefficient) for the polarizer Faraday cell,* wavelengths 400 to 700 nm.

Fig. 3 Schematic of film models investigated for the interpretation of spectroscopic ellipsometer measurements of thin Pb deposits on Cu substrates. Number of adjustable parameters given in parentheses. (a) compact single film (1); (b) porous single film, optical constants of effective medium determined according to Maxwell-Garnett (2) or Bruggeman (2); (c) island single film, reflection coefficient determined by coherent superposition of polarization states, islands compact (2), porous (3) or anisotropic (6); (d) multilayer films, three layers: compact and porous layers, dendritic islands (6) or two layers: compact and porous films (3).

Fig. 4. Spectroscopic simulations for compact film model (solid lines) Pb deposits of thickness 0, 1, 5, 10, 20, 31, 60, 110 nm. Experimental measurements (dotted lines) for 31, 60, 110 nm equivalent compact Pb deposits (based upon coulometric measurements) on Cu.

---

*SF6 cores

Fig. 5. Spectroscopic simulations of porous film model (solid lines) Volume fractions of Pb 0.1 to 0.9, amount of deposit corresponding to a 31 nm compact Pb layer on a Cu substrate. Simulations based upon the effective medium approximation (Bruggeman eq.). Experimental measurements (dotted lines) for 0 and 31 nm equivalent compact film.

Fig. 6. Spectroscopic simulations of island film model (solid lines). Surface coverage 0.1 to 1.0, amount of deposit corresponding to 31 nm compact layer, Cu substrate. Simulations based on coherent superposition of polarization states. Experimental measurements (dotted lines) for 0 and 31 nm equivalent compact film.

Fig. 7. Spectroscopic simulation for optimum fit of ellipsometer parameter delta for a two-layer film model (circles) and measurements (solid lines) for equivalent deposit thicknesses of 0, 31, 60 and 110 nm. Film parameters derived from optimum fit of model predictions to measurements given in Table II.

Fig. 8. Spectroscopic simulation for optimum fit of ellipsometer parameter psi for a two-layer film model; other comments as in Fig. 7.

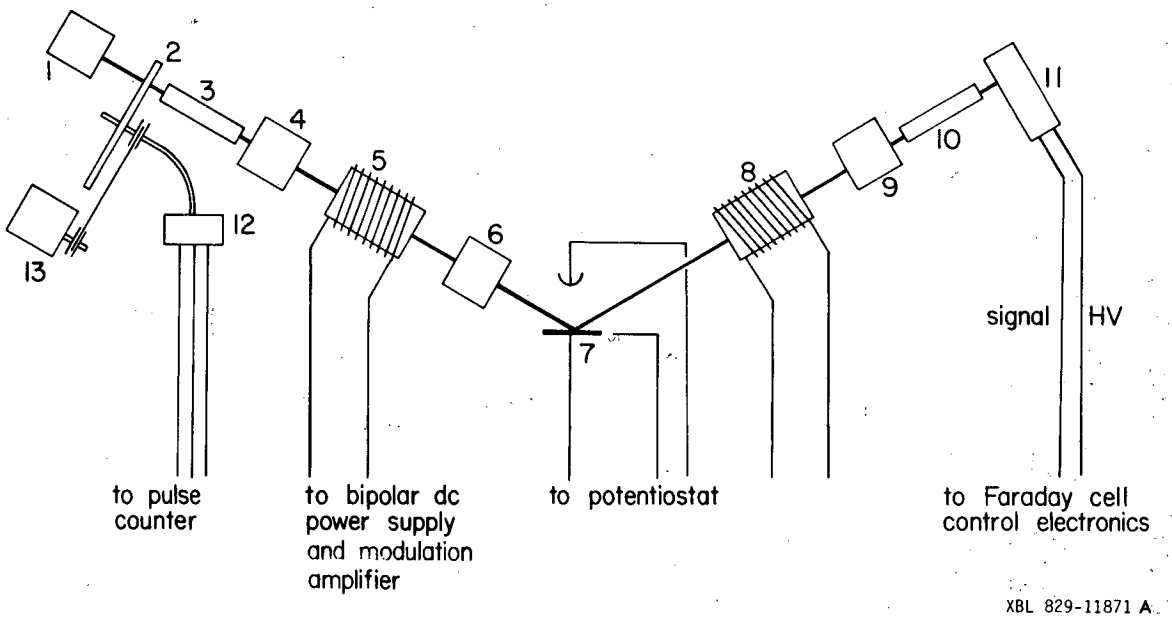
1
2
3
4
5
6
7
8
9
10
11
12
13
signal
HV
to pulse counter
to bipolar dc power supply and modulation amplifier
to potentiostat
to Faraday cell control electronics
XBL 829-11871 A

Fig. 1

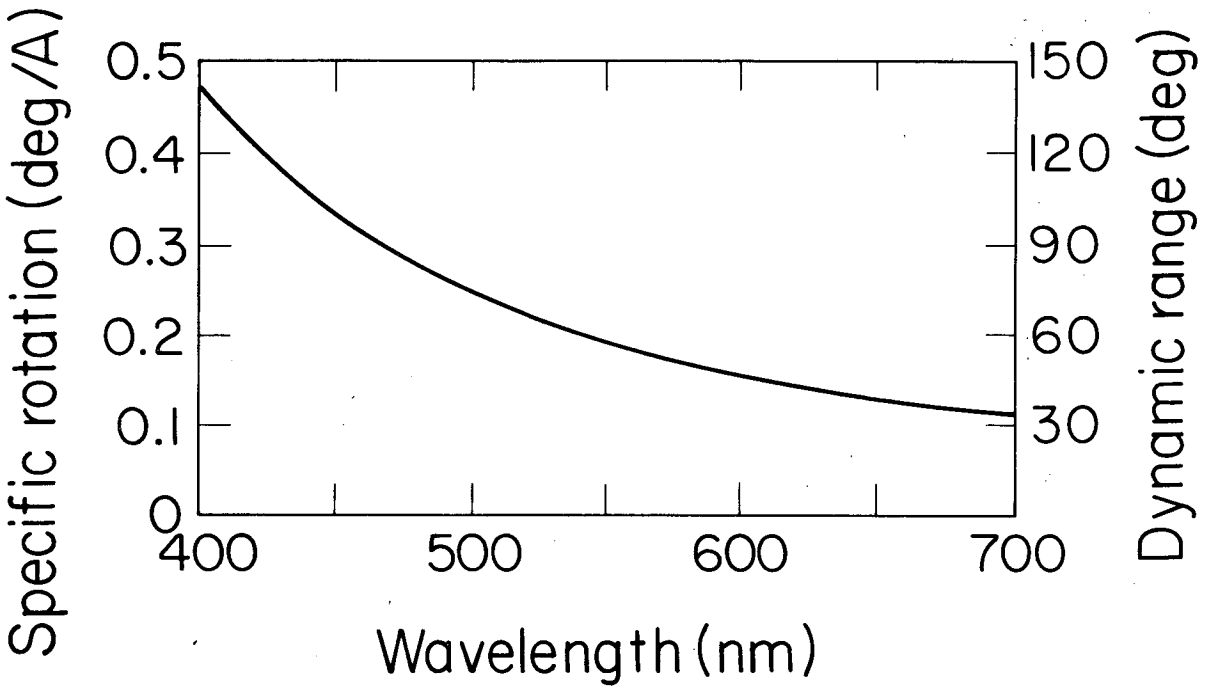

XBL 834-1202B

Fig. 2

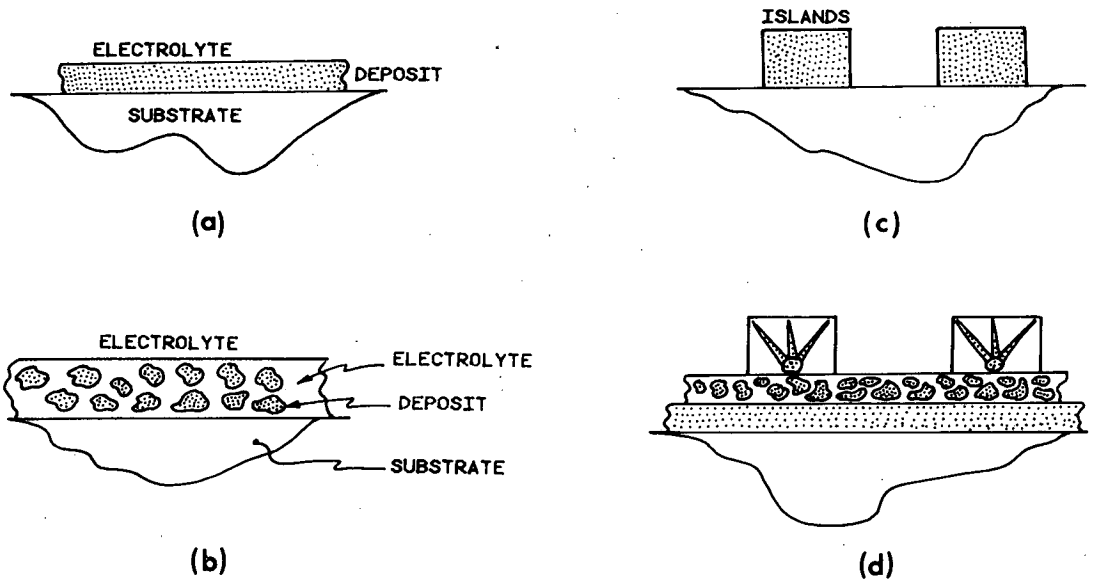

XBL 829-11873 A

Fig. 3

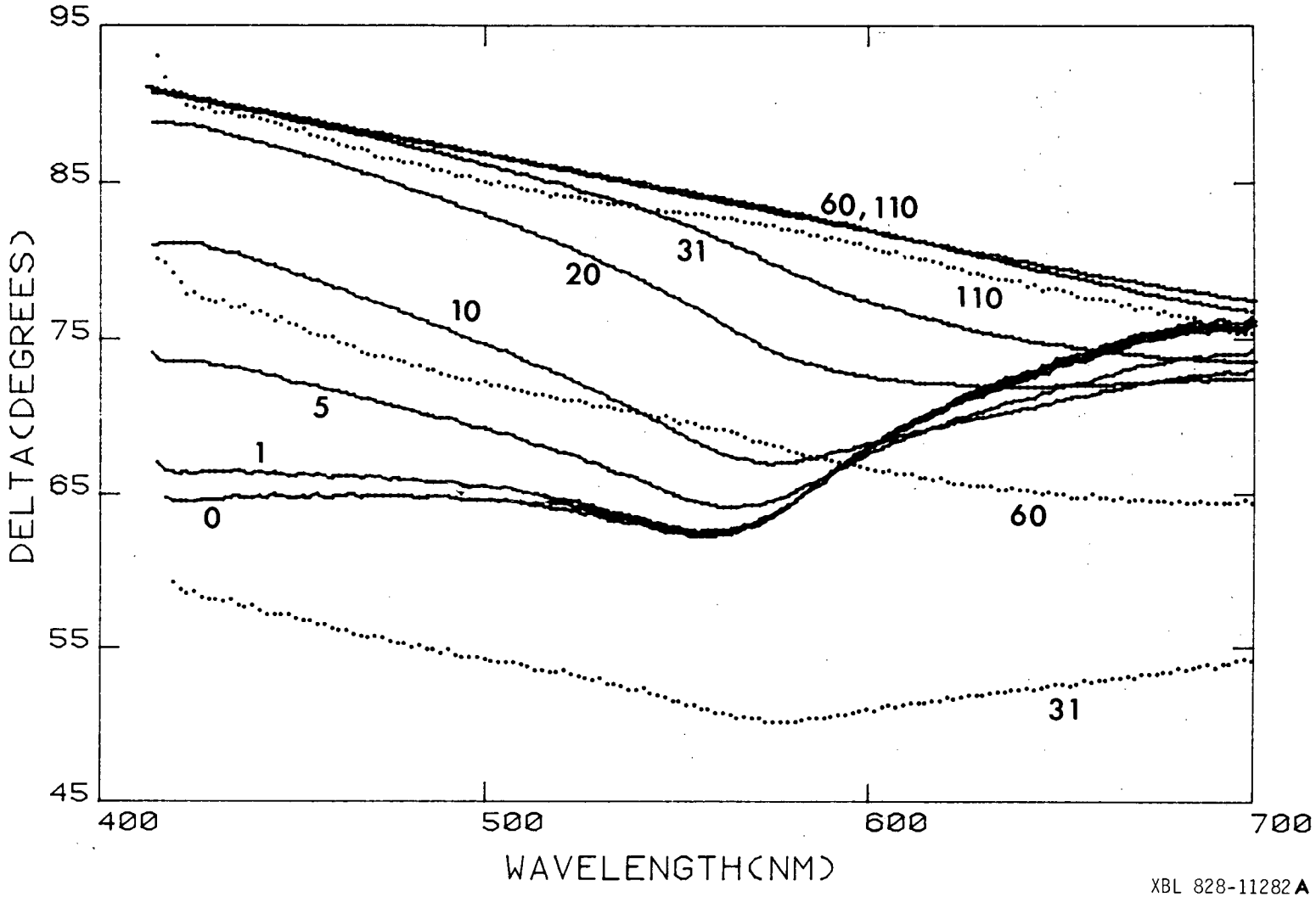

XBL 828-11282A

Fig. 4

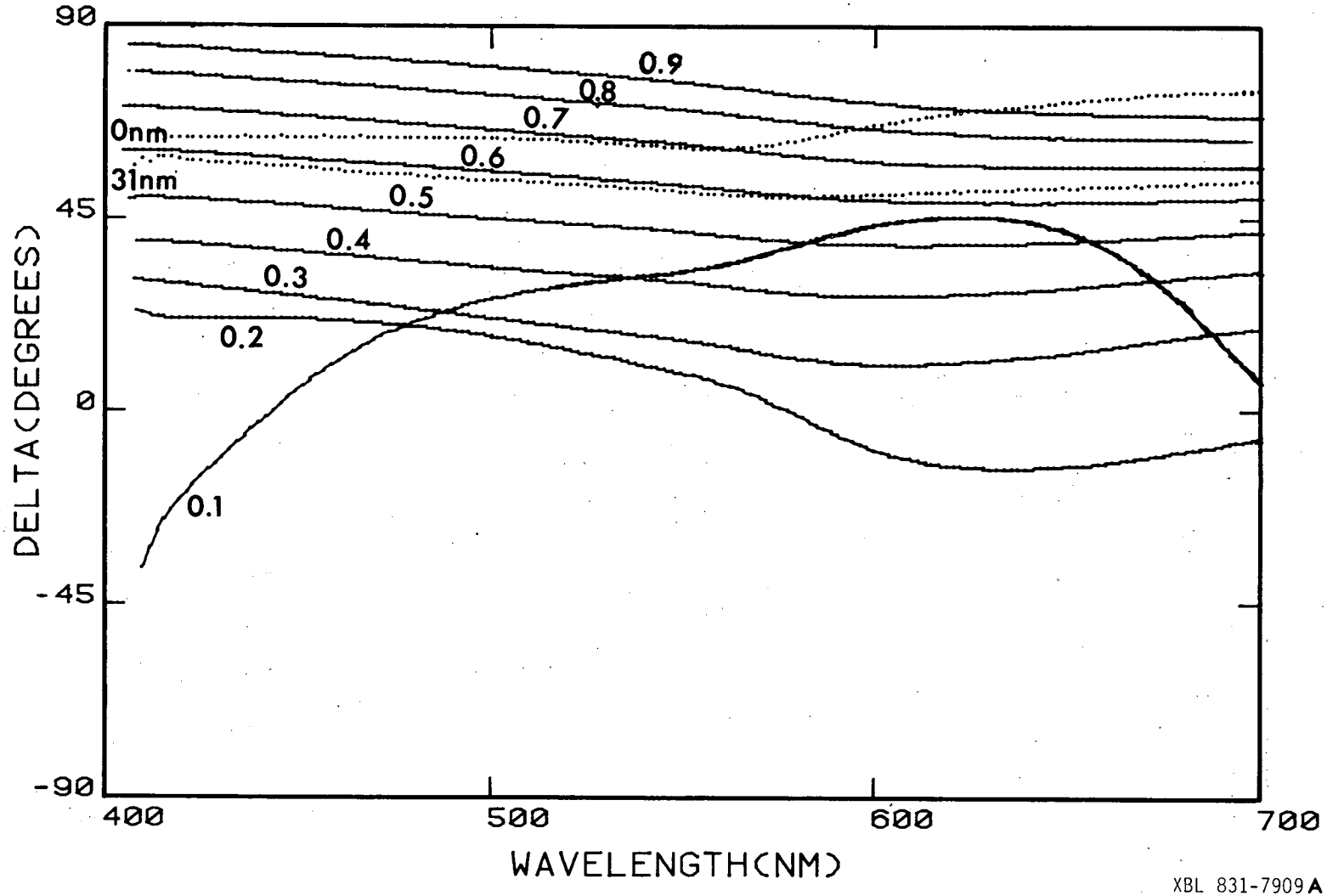

XBL 831-7909A

Fig. 5

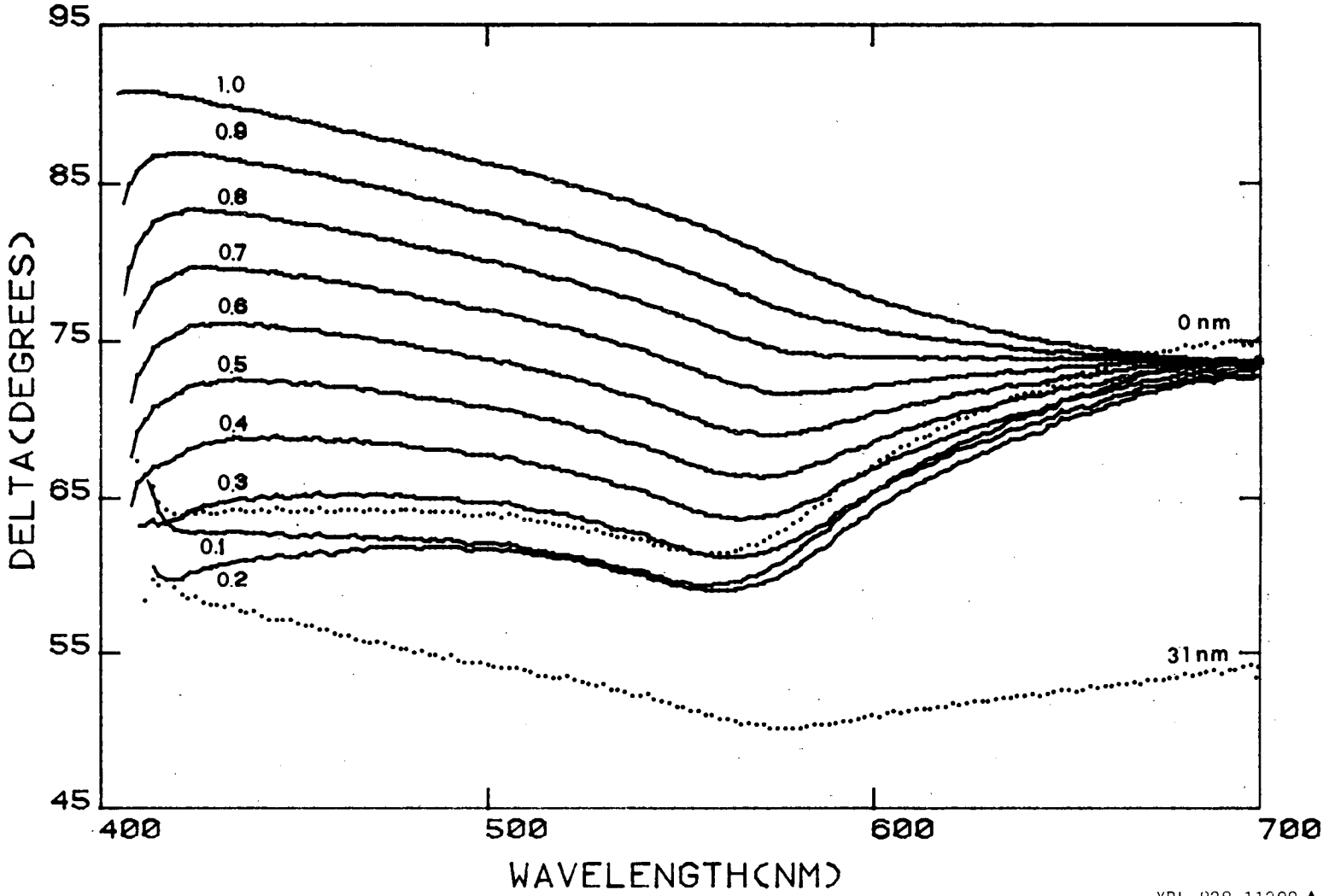

XBL 828-11288 A

Fig. 6

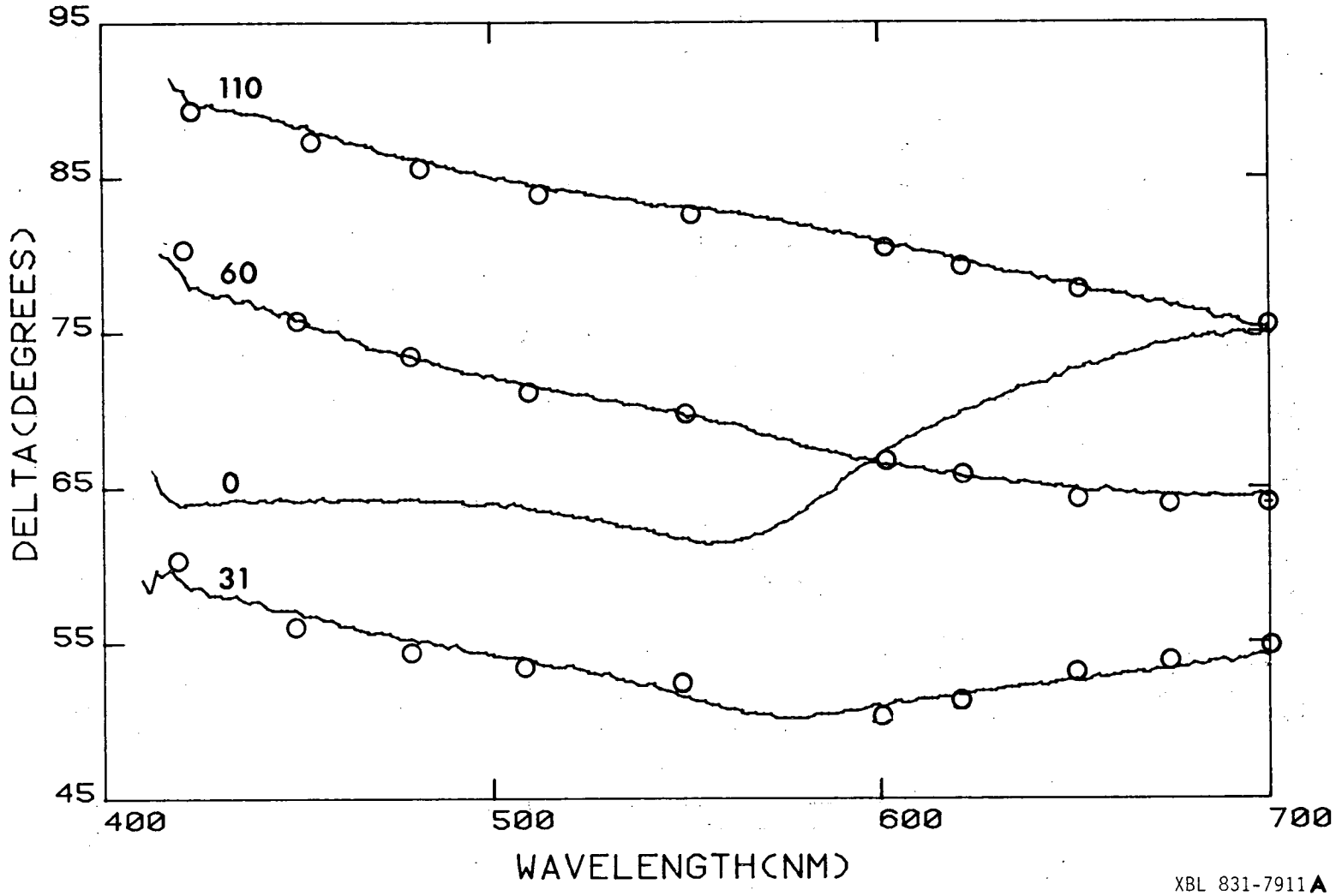

XBL 831-7911A

Fig. 7

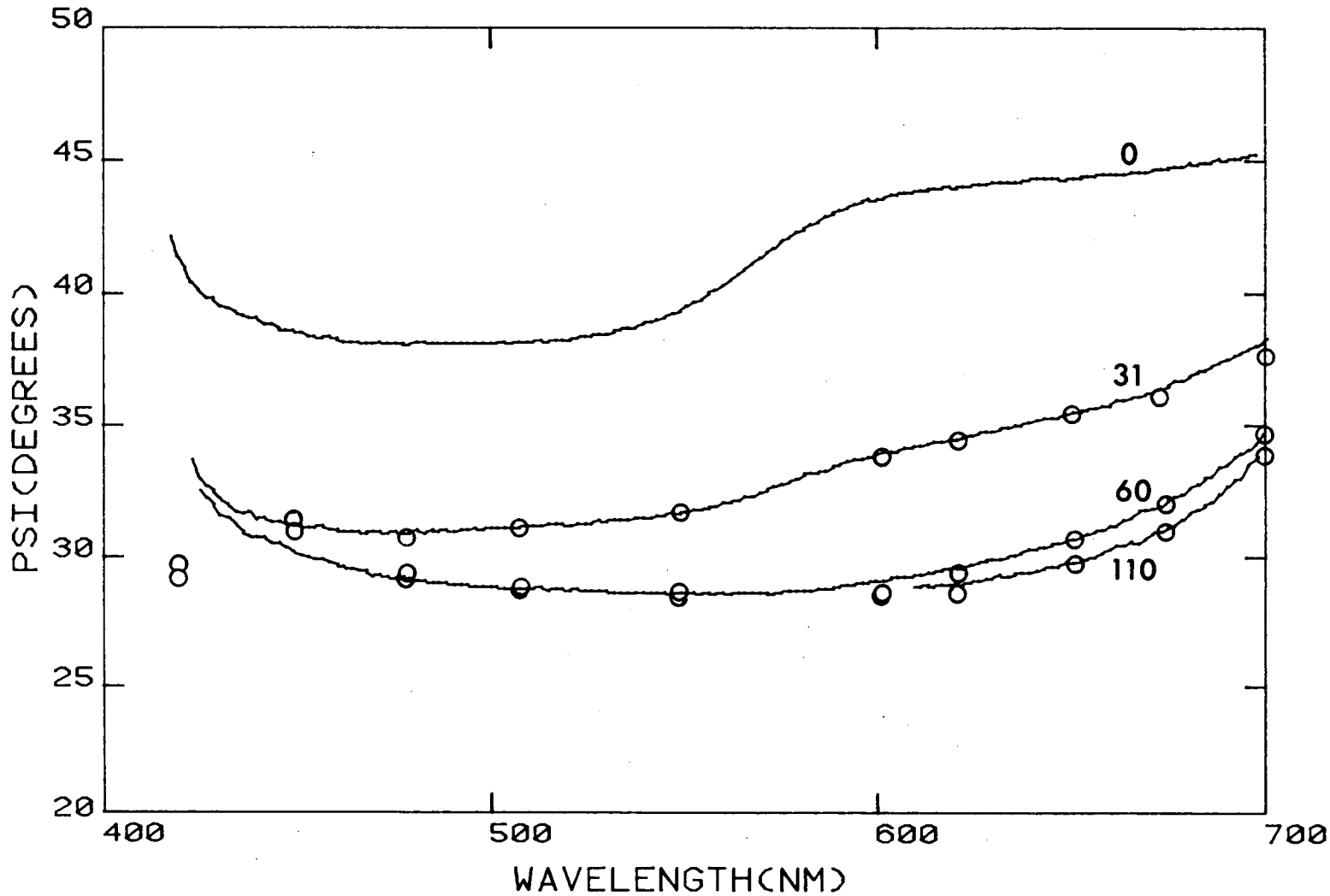

XBL 831-7912 A

Fig. 8

This report was done with support from the Department of Energy. Any conclusions or opinions expressed in this report represent solely those of the author(s) and not necessarily those of The Regents of the University of California, the Lawrence Berkeley Laboratory or the Department of Energy.

Reference to a company or product name does not imply approval or recommendation of the product by the University of California or the U.S. Department of Energy to the exclusion of others that may be suitable.

TECHNICAL INFORMATION DEPARTMENT
LAWRENCE BERKELEY LABORATORY
UNIVERSITY OF CALIFORNIA
BERKELEY, CALIFORNIA 94720